IJMMM International Journal of Minerals, Metallurgy and Materials 矿物冶金与材料学报（英文版）

Comprehensive utilization of complex rubidium ore resources: Mineral dissociation and selective leaching of rubidium and potassium

Quankuang Zhang, Baozhong Ma, Chengyan Wang, Yongqiang Chen, and Wenjuan Zhang

Cite this article as:
Quankuang Zhang, Baozhong Ma, Chengyan Wang, Yongqiang Chen, and Wenjuan Zhang, Comprehensive utilization of complex rubidium ore resources: Mineral dissociation and selective leaching of rubidium and potassium, *Int. J. Miner. Metall. Mater.*, 30(2023), No. 5, pp. 857-867. https://doi.org/10.1007/s12613-022-2436-1

International Journal of Minerals, Metallurgy and Materials
Volume 30, Number 5, May 2023, Page 857
https://doi.org/10.1007/s12613-022-2436-1

Comprehensive utilization of complex rubidium ore resources: Mineral dissociation and selective leaching of rubidium and potassium

Quankuang Zhang[1,2], *Baozhong Ma*[1,2),✉], *Chengyan Wang*[1,2),✉], *Yongqiang Chen*[1,2)], *and Wenjuan Zhang*[1,2)]

1) State Key Laboratory of Advanced Metallurgy, University of Science and Technology Beijing, Beijing 100083, China
2) School of Metallurgical and Ecological Engineering, University of Science and Technology Beijing, Beijing 100083, China
(Received: 3 December 2021; revised: 9 February 2022; accepted: 11 February 2022)

Abstract: Currently, the process of extracting rubidium from ores has attracted a great deal of attention due to the increasing application of rubidium in high-technology field. A novel process for the comprehensive utilization of rubidium ore resources is proposed in this paper. The process consists mainly of mineral dissociation, selective leaching, and desilication. The results showed that the stable silicon–oxygen tetrahedral structure of the rubidium ore was completely disrupted by thermal activation and the mineral was completely dissociated, which was conducive to subsequent selective leaching. Under the optimal conditions, extractions of 98.67% Rb and 96.23% K were obtained by leaching the rubidium ore. Moreover, the addition of a certain amount of activated $Al(OH)_3$ during leaching can effectively inhibit the leaching of silicon. In the meantime, the leach residue was sodalite, which was successfully synthesized to zeolite A by hydrothermal conversion. The proposed process provided a feasible strategy for the green extraction of rubidium and the sustainable utilization of various resources.

Keywords: rubidium; mineral dissociation; selective leaching; zeolite A; desilication

1. Introduction

Rubidium is a soft, active, and rare metal with unique optoelectronic properties and has been widely used in traditional fields such as atomic clocks, photovoltaic cells, special glasses, biochemistry, and medicine [1–3]. In particular, with the rapid development of rubidium in emerging applications such as magnetic fluid power generation, thermal ion conversion power generation, and ion propulsion engine, the demand of rubidium has also grown significantly year by year [4–6]. Although rubidium is ranked 16th in abundance in the earth's crust, rubidium has no independently occurring mineral and is mainly found in feldspar and mica in the form of isomorphism by replacing the position of potassium [7–8]. For a long time, rubidium was extracted mainly from lepidolite ($(K,Rb)Li_2AlSi_4O_{10}F_2$) and pollucite ($Cs_2Al_2Si_4O_{12}$) as a byproduct of lithium and cesium extraction [9]. The annual production of rubidium worldwide is only 2–4 t [10].

Rubidium has been found to be concentrated in ores and brines [10–12]. Although brines account for more than 90% of the total reserves, rubidium usually is found in trace concentrations (0–20 mg/L), which makes it costly and technically difficult to extract [13–14]. As a result, the current study of rubidium extraction technology has focused on the extraction of rubidium from ores. In general, rubidium ores are currently treated mainly by roasting decomposition and acid decomposition [15–16]. The principle of roasting is the decomposition of alkali metal or alkaline earth metal chlorides at high temperatures (800–900°C) with water to produce hydrogen chloride gas [17]. The rubidium in it is converted into soluble rubidium chloride by the reaction of hydrogen chloride with mica, which is then recovered by water leaching [18]. Although high extraction rate of rubidium can be obtained by chlorination roasting and water leaching, the current studies have only considered the recovery of rubidium, resulting in a low level of comprehensive resource utilization. In addition, chlorination roasting often produces a large amount of waste gas containing hydrogen chloride, which will bring a series of problems, such as poor operating environment, higher cost of waste gas treatment,, and equipment corrosion [18–19].

Mica and feldspar are generally considered to be natural rubidium resources and both are composed primarily of stable silica–oxygen tetrahedral structures [20–21]. Therefore, the destruction of the stable silicon–oxygen tetrahedral structure is a prerequisite to obtaining high extraction rate of rubidium. According to geochemical studies, mica is susceptible to acidic erosion and feldspar to alkaline erosion, but the efficiency of atmospheric pressure leaching is too low [22–24]. Studies demonstrate that enhanced leaching processes are more competitive than roasting processes in ore extraction metallurgy [25–26]. A process for the leaching of

✉ Corresponding authors: Baozhong Ma E-mail: bzhma_ustb@yeah.net; Chengyan Wang E-mail: chywang@yeah.net

strong acids has been proposed and systematically investigated by Lou *et al.* [27]. Although the stable silica-oxygen tetrahedral structure in mica could be efficiently destroyed under enhanced acid leaching conditions, the sulfuric acid was inefficient and could not be regenerated, resulting in a large amount of acid-containing wastewater that was difficult to treat [28–30]. Beside, some researchers conducted alkali leaching of feldspar and mica in autoclave by intensifying the leaching conditions [20,31–32]. The enhanced alkali leaching not only resulted in a high leaching rate but also avoided the generation of large amounts of waste gas and wastewater [33]. However, the intensive alkali leaching process also had the problems with high leaching pressure and high alkali consumption [34]. If the leaching pressure and alkali consumption are further reduced, it is of great importance for the technological development of rubidium extraction from ores by alkaline leaching.

In this paper, a novel method for the comprehensive utilization of complex rubidium ore resources was proposed, and the process not only took into account the efficient recovery of rubidium but also achieved a high-value utilization of the abundant silicon and aluminum resources. The technical route for the comprehensive utilization of complex rubidium resources consists mainly of the following steps: (1) dissociation of stable mineral structures in rubidium ore, (2) selective leaching of the thermal activated slag (Slag-1), and (3) desilication of alkaline leaching solutions with aluminum hydroxide and zeolite synthesis. The effects of various parameters on extraction efficiency were systematically investigated during thermal activation and selective leaching. The results of the study will provide theoretical and technological support for the low-cost, efficient, and clean utilization of Rb-bearing minerals.

2. Experimental

2.1. Materials

The rubidium ore was finely ground to below 74 μm by a vibration mill prototype. Table 1 presents the chemical composition of rubidium ore. NaOH and $Al(OH)_3$ were purchased from Beijing Honghu Lianhe Huagong Chanpin Co., Ltd., China. All chemical agents were analytical pure grade.

Table 1. Chemical composition of the rubidium ore wt%

Rb	SiO_2	Al	K	Fe	Ca	Mg	C	F
0.16	58.07	9.20	5.41	5.65	0.68	0.38	0.18	1.66

2.2. Apparatuses and procedure

The rubidium ore with a certain amount of NaOH was thoroughly mixed and subsequently roasted in a silicon–molybdenum furnace at a pre-determined temperature and time. After reaching the pre-determined holding time, the roasted sample was directly taken out and poured into cold water for rapid cooling. The Slag-1 was finally leached in a beaker after fine grinding. To determine the optimal mineral dissociation conditions, the selective leaching conditions (initial NaOH concentration, liquid-to-solid ratio (L/S), temperature (T), and leaching time (t)) were set at 150 g/L, 5 mL/g, 95°C, and 2 h. After the leaching was completed, the leaching residue was washed several times (2 to 3 times) to ensure that the residual NaOH was washed away. The leaching residue after washing was dried at 80°C for 24 h. Finally, a certain amount of activated $Al(OH)_3$ was added to the leaching liquor for desilication, which was also performed in a beaker.

2.3. Analysis methods

Metals in rubidium ore, leaching, solution, and desilication slag (Slag-2) were analyzed by inductively coupled plasma-optical emission spectroscopy (ICP-OES; 8300 PerkinElmer, America). The mass loss and heat change of the materials were analyzed through thermogravimetry–differential scanning calorimetry (TG–DSC). The phase of the solid particles was analyzed using X-ray diffractometer (XRD; Ultima IV Japanese Science, Japan). The particle size distribution of the ore sample was tested by a laser particle sizer (Mastersizer 3000, China). The microstructure and main elements distribution of the solid particles were analyzed through scanning electron microscopy (SEM; SUPRA55, Zeiss, Germany) and energy dispersive X-ray spectroscopy (EDS; EDAX, Germany). The silicon in solution was also analyzed using ICP-OES.

3. Results and discussion

3.1. Characterization of the rubidium ore

The particle size distribution of rubidium ore was measured, as shown in Fig. 1(a). It can be seen that the D_{50} particle size of the rubidium ore was 9.47 μm, and the D_{90} was 46 μm (D_{10}, D_{50}, and D_{90} represent the particle size at 10%, 50%, and 90% of the particle size distribution, respectively). The XRD pattern of the rubidium ore is shown in Fig. 1(b). The main material phases were identified as quartz, feldspar, and mica.

Combined with SEM–EDS (Fig. 2), rubidium was present both in feldspar and mica in the form of isomorphism [20]. The deposit state of rubidium and potassium made it difficult to process efficiently by conventional processes. Therefore, the destruction of feldspar and mica structures was an essential prerequisite for the efficient extraction of rubidium and potassium.

3.2. Mineral dissociation

Fig. 3 shows the TG–DSC curves for the raw ore and the raw ore mixed with NaOH (a ratio of NaOH to ore of 30wt%). The TG–DSC of rubidium ore showed that three endothermic peaks and mass loss occur with the gradual increase in temperature: the first peak in the 529°C regions was most likely to be the dehydroxylation of kaolinite [35], the peak at 1068°C corresponded to the mineral starting to melt (Table S1), whereas the third peak at 1275°C was caused by a glass phase transition of the mineral. Notably, when the raw ore was mixed with 30wt% NaOH, there was an additional heat absorption peak at 790°C accompanied by a significant mass loss, which was most likely due to the reaction of the

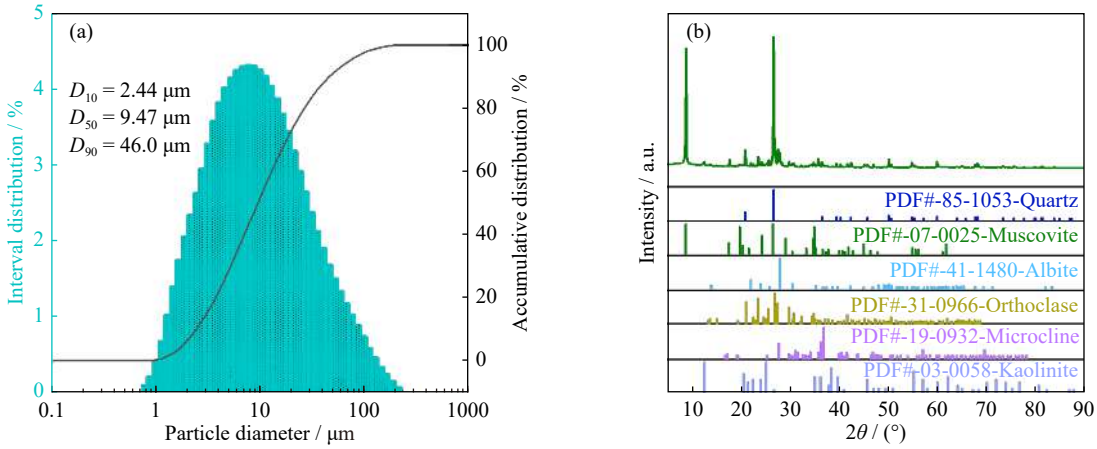

Fig. 1. Characterization of the rubidium ore: (a) particle size distribution and (b) XRD pattern.

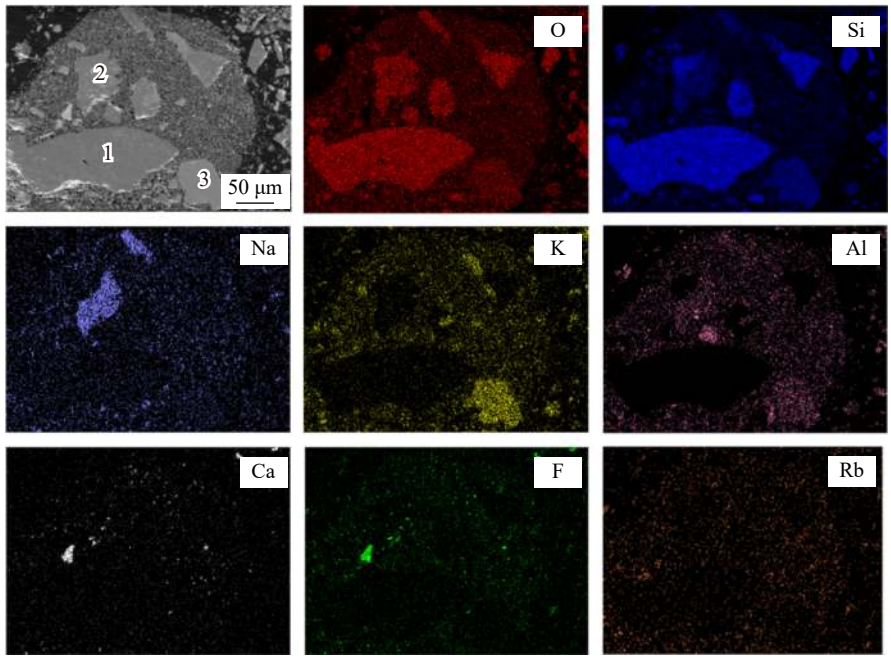

Fig. 2. SEM image and EDS maps of the rubidium ore (1—Quartz; 2—Mica; 3—K-feldspar).

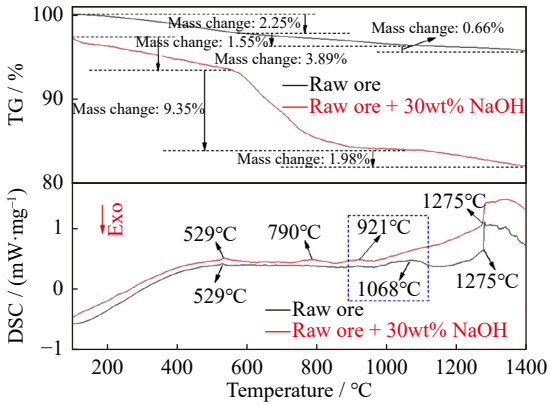

Fig. 3. TG–DSC curves of raw ore and raw ore mixed with 30wt% NaOH.

mineral with NaOH, releasing water vapour, as shown in Eqs. (1) and (2) [20].

$$6KAlSi_3O_8 + 18NaOH = 3Na_2Al_2Si_3O_{10} + 3K_2SiO_3 + 6Na_2SiO_3 + 9H_2O\uparrow \quad (1)$$

$$6KAlSi_3O_8 + 24NaOH + 2CaCO_3 = Na_6Ca_2(Al_6SiO_{24}(CO_3)_2) + 3K_2SiO_3 + 9Na_2SiO_3 + 12H_2O\uparrow \quad (2)$$

Interestingly, the glass phase transition temperature of the material after mixing the raw ore with 30% NaOH remained unchanged and the starting melting temperature of the mixture was reduced to 921°C, which was 147°C lower than when NaOH was not added. The results of the thermogravimetric analysis indicated that the addition of NaOH during the dissociation stage would probably be more favorable to the dissociation of the minerals and effectively increase the Slag-1 activity. Therefore, the effects of the mass ratio of NaOH to ore, temperature, and roasting time were mainly investigated during the mineral dissociation stage.

3.2.1. Effect of mass ratio of NaOH to ore

Combined with the results of the previous analysis of the thermogravimetric curves (Fig. 3), the glass phase transition of rubidium ore would only occur at 1275°C and the addition of NaOH would not alter the glass phase transition temperat-

ure of the mineral. Therefore, to adequately destroy the mineral structure, the dissociation temperature and time were set at 1300°C and 2 h, respectively, when exploring the effect of NaOH addition. Without the addition of NaOH, the leaching activity of the Slag-1 was low (Fig. 4(a)), and extraction rate of rubidium was only approximately 50%. The leaching rate of rubidium was effectively improved after NaOH was added. In particular, the maximum leaching rate of rubidium was obtained when the addition of NaOH was 25wt%. Considering that by continuing to increase the amount of NaOH, the metal extraction no longer increased and the extra NaOH would inevitably absorb gases such as CO_2, making the byproduct Na_2CO_3 increase, which would not only cause a waste of resources but also make the leachate composition more complex. Therefore, 25wt% was chosen as the optimum addition amount of NaOH.

3.2.2. Effect of dissociation temperature

The dissociation temperature was also an important factor in the activity of the Slag-1. Fig. 4(b) demonstrates the effect on the leaching activity of the Slag-1 at dissociation temperatures in the range from 1200 to 1400°C. The leaching rates of rubidium and potassium were relatively low at 1200°C (65% and 52%) and increased gradually as the dissociation temperature increased. At 1250°C, the maximum leaching rate of rubidium reached 86%, but the leaching rate of potassium continued to increase with the dissociation temperature and stabilized at 1300°C. Consequently, 1300°C was chosen as the optimum dissociation temperature in subsequent experiments. Combined with the thermogravimetric curve analysis results of the rubidium ore in Fig. 3, the glass phase transition of the mineral occurred at 1275°C. The mineral was completely transformed into a highly active amorphous state at 1300°C. This was also the reason for the highest activity of the Slag-1 obtained at 1300°C.

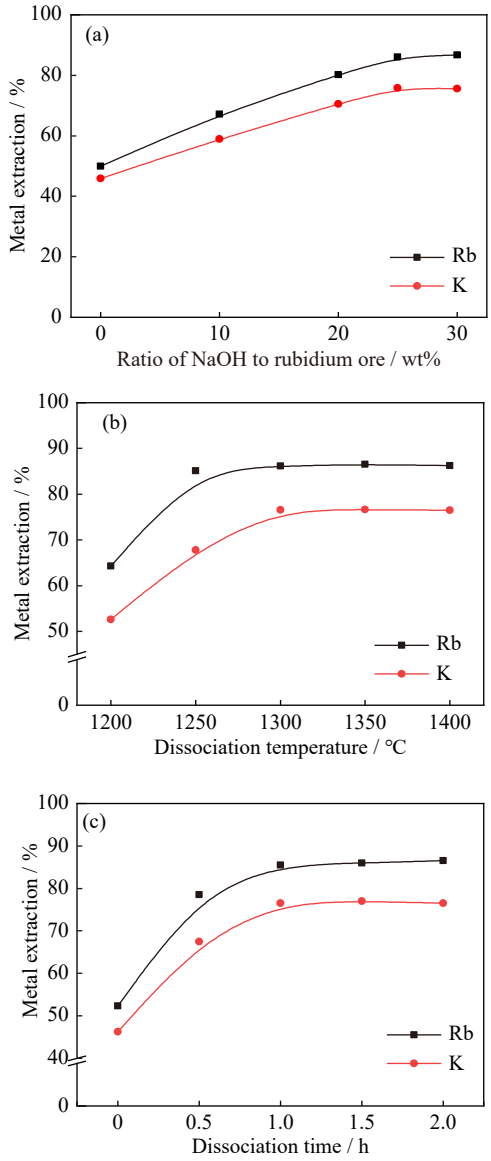

Fig. 4. Effects of (a) ratio of NaOH to rubidium ore, (b) dissociation temperature, and (c) dissociation time on the extraction of Rb and K (Leaching conditions: T = 95°C, NaOH = 150 g/L, L/S = 5 mL/g, and t = 2 h).

3.2.3. Effect of dissociation time

The effect of dissociation time on the activity of the Slag-1 is shown in Fig. 4(c). When the holding time was too short, the leaching activity of the Slag-1 was low, which was due to the glass phase transformation of the minerals was incomplete and most of them still existed in a stable state. When the holding time reached 1 h, the leaching rates of rubidium and potassium were 86% and 77%, respectively. By continuing to increase the dissociation time, the leaching rate of rubidium and potassium hardly increased anymore, so 1 h was chosen as the optimum dissociation holding time.

Through systematic experiments, the optimum mineral dissociation conditions were determined: a ratio of NaOH to ore of 25wt%, a dissociation temperature of 1300°C, and a dissociation time of 1 h. The Slag-1 was further analyzed using SEM–EDS mapping to compare the distribution of the main elements after mineral dissociation. The SEM–EDS images of the raw ore (Fig. 2) showed that rubidium was only distributed centrally in the feldspar and mica. However, when the raw ore was dissociated by mineral activation at high temperatures, rubidium was released and all elements were present in a highly dispersed state (Fig. 5), achieving complete dissociation of the mineral. The high activity of Slag-1 also provided the basis for the efficient extraction of rubidium and potassium in the selective leaching process.

3.3. Selective leaching

First, to further predict the decomposition behavior of the Slag-1 in lye and the possible presence of the material phases, the phase diagram of the K_2O–Al_2O_3–SiO_2–Na_2O system was plotted by the FactPS, and FToxid databases in the Phase Diagram module of the FactSage7.0 thermodynamic software. As shown in Fig. 6, based on the composition of the Slag-1, the stable phases in the phase diagram were nepheline ($KNa_3[AlSiO_4]_4$), Na_2SiO_3, K_2SiO_3, and $NaAlO_2$ for a range of possible experimental conditions.

It should be noted that secondary reactions could occur between Na_2SiO_3, K_2SiO_3, and $NaAlO_2$ at different leaching times, alkali concentrations, and temperatures to produce different types of zeolites. Fig. 6 also shows that changes in leachate base concentration can have a large effect on the phases in solution.

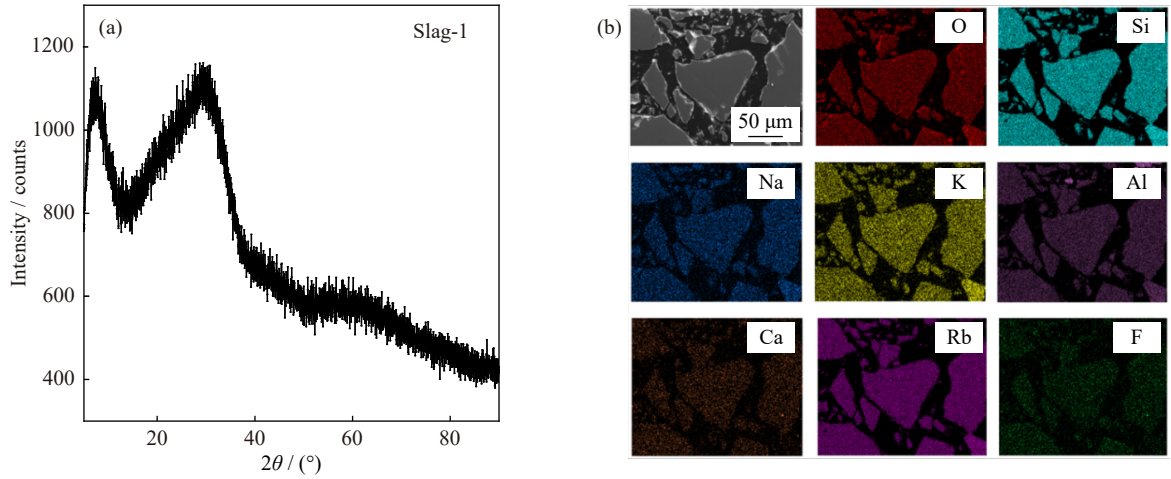

Fig. 5. (a) XRD pattern and (b) SEM image and EDS maps of the slag-1 under the optimum mineral dissociation conditions.

3.3.1. Effect of initial NaOH concentration

Based on the results of the Factsage software calculations in Fig. 6, it can be concluded that the NaOH concentration significantly affects the leaching process. Therefore, the influence of different initial NaOH concentrations on the leaching of rubidium and potassium was further investigated. The temperature, liquid-to-solid ratio, leaching time, and stirring rate were maintained at 90°C, 5 mL/g, 2 h, and 400 r/min, respectively. As shown in Fig. 7(a), the leaching rates of both rubidium and potassium increased continuously with increasing initial NaOH concentration. When the initial concentration of NaOH was 200 g/L, the leaching rates of rubidium and potassium reached a plateau, which were 96.45% and 90.57%, respectively. Therefore, the optimum initial NaOH concentration was chosen to be 200 g/L for following leaching.

As shown in Fig. 8, when the initial concentration of NaOH was below 100 g/L, the leaching residue was still an

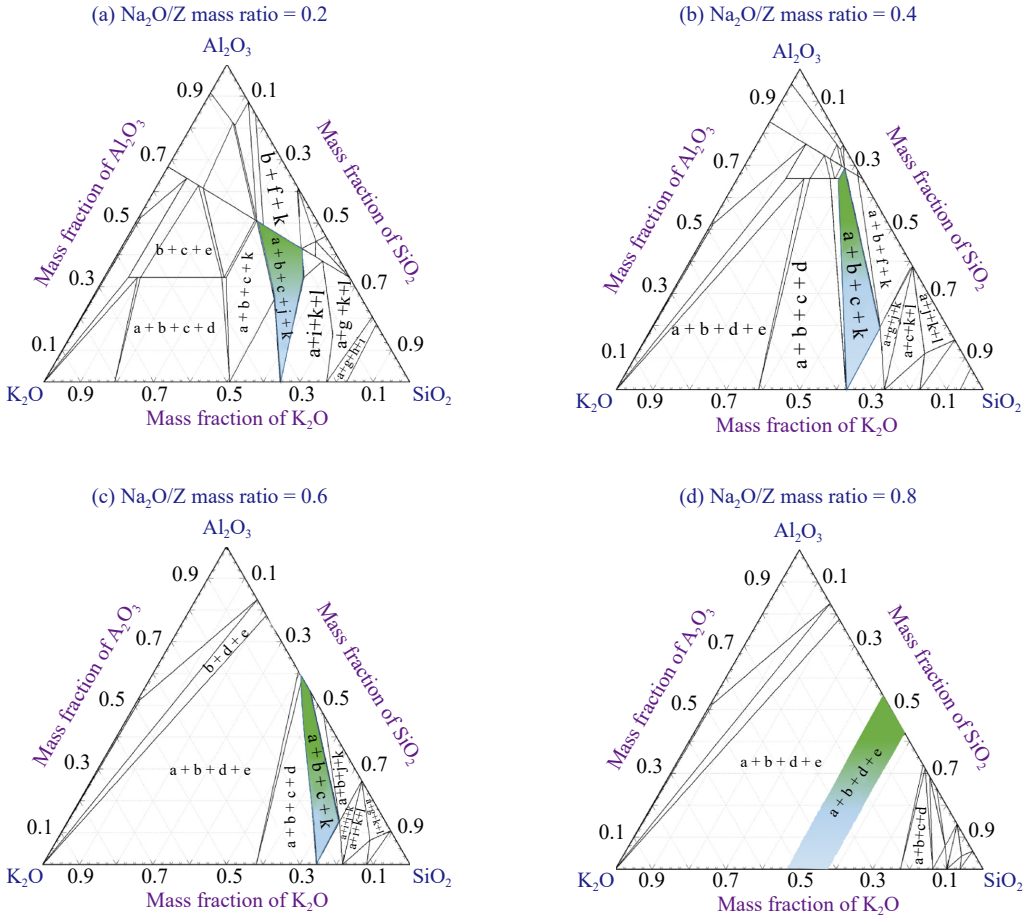

Fig. 6. Phase diagram of the K_2O–Al_2O_3–SiO_2–Na_2O–H_2O system (Na_2O/Z = 0.2, 0.4, 0.6, and 0.8 in mass ratio, H_2O/Z = 5 in mass ratio, Z = (Al_2O_3 + SiO_2 + K_2O), 90°C, and 101.325 kPa). a—Na_2SiO_3; b—$NaAlO_2$; c—K_2SiO_3; d—KOH; e—NaOH; f—$KAlSiO_4$; g—$NaAlSi_3O_8$; h—$K_2Si_4O_9$; i—$K_2Si_2O_5$; j—$NaAlSiO_4$; k—Nepheline; l—Feldspar.

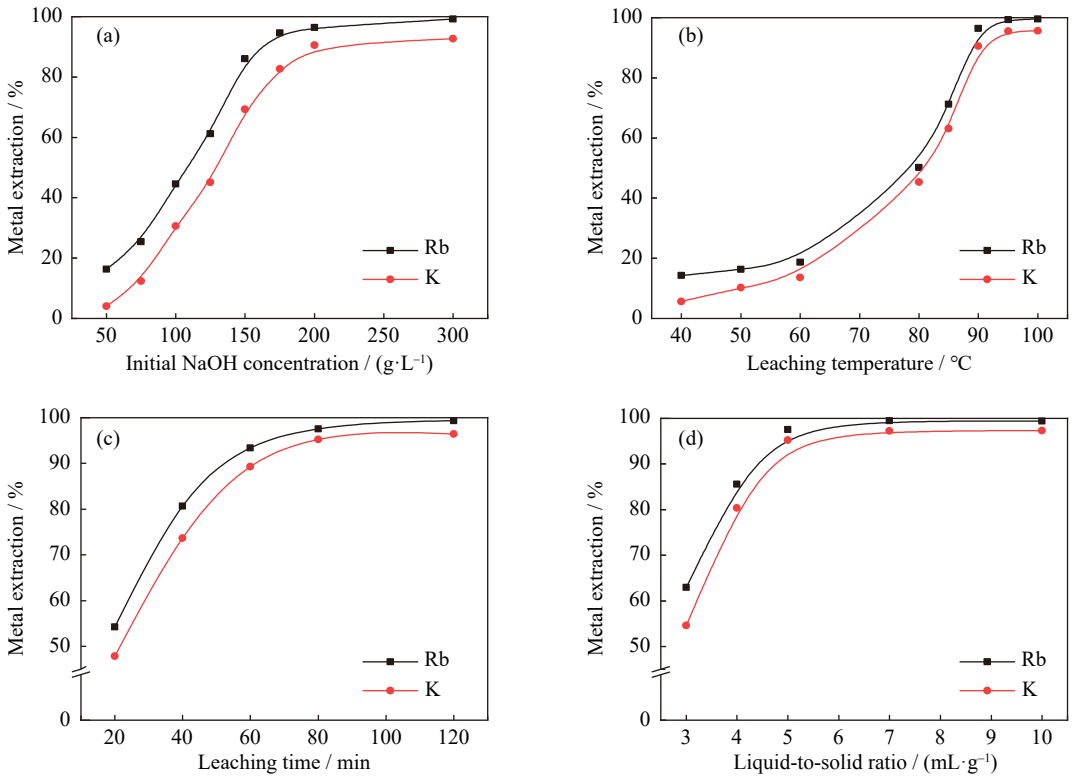

Fig. 7. Effects of (a) initial NaOH concentration, (b) leaching temperature, (c) leaching time, and (d) liquid-to-solid ratio on the extraction of Rb and K (Mineral dissociation conditions: a ratio of NaOH to ore of 25wt%, a dissociation temperature of 1300°C, and a dissociation time of 1 h).

amorphous form and the corresponding metal leaching rates were relatively low. When the initial concentration of NaOH reached 125 g/L, the leaching residue began to change from an amorphous state to a crystalline state, and zeolite A phase appeared. Interestingly, as the initial NaOH concentration continued to increase to 150 g/L, a new phase (sodalite) began to appear in the leaching residue, but at this point zeolite A was still the dominant phase. Thereafter, as the initial NaOH concentration continued to increase, zeolite A phase eventually disappeared and sodalite became the predominant phase in the leaching residue. Accordingly, the conversion of zeolite A to sodalite during leaching depends on the initial NaOH concentration. This result was in agreement with the calculation results of Factsage software in Fig. 6 and the conversion mechanism of zeolite A to sodalite [36–37].

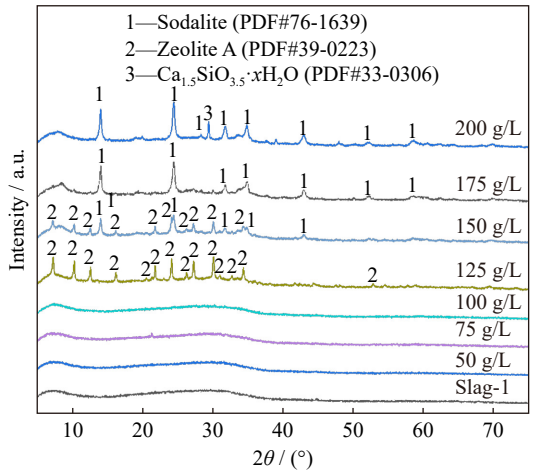

Fig. 8. XRD patterns of the leach residue at various NaOH concentrations.

3.3.2. Effect of leaching temperature

Temperature is a significant factor in chemical reactions and increasing the temperature of metals extracted from minerals not only increases the rate of reaction but also promotes the decomposition and transformation of the mineral phase [38–39]. Fig. 7(b) demonstrates the effect of different leaching temperatures on metal extraction rates. The initial NaOH concentration, liquid-to-solid ratio, leaching time, and stirring rate were maintained at 200 g/L, 5 mL/g, 2 h, and 400 r/min, respectively. It was clear that the leaching rates of rubidium and potassium increased more slowly with increasing temperature when the temperature was below 80°C. However, the leaching rates of rubidium and potassium increased rapidly with increasing temperatures above 80°C. The leaching rate of the metals reached stability at 95°C, so the optimum leaching temperature was chosen to be 95°C.

XRD analysis of the leaching residue was carried out to investigate the phase transformation of the Slag-1 at different temperatures. It can be seen from Fig. 9 that when the temperature was below 85°C, no peaks appeared in the XRD pattern and the leaching residue was still present in an amorphous state. As the leaching temperature increased above 85°C, the sodalite phase gradually appeared in the leaching residue and the intensity of sodalite peaks increased with temperature. Eventually, sodalite and a small amount of hydrated calcium silicate became the main phases of the leaching residue as the temperature increased further.

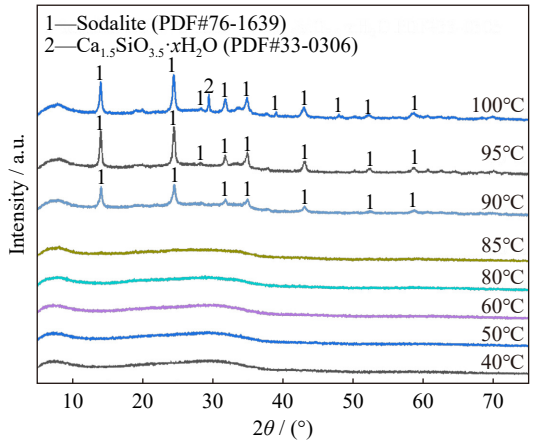

Fig. 9. XRD patterns of the leaching residue at various leaching temperatures.

3.3.3. Effect of leaching time

Extending the leaching time could effectively increase the extraction rate of metals. Hence, the effect of leaching time on the leaching rates of rubidium and potassium was investigated. Constant conditions included an initial NaOH concentration of 200 g/L, leaching temperature of 95°C, liquid-to-solid ratio of 5 mL/g, and stirring rate of 400 r/min. As shown in Fig. 7(c) the extraction rates of rubidium and potassium reached 80.67% and 73.64% respectively at a reaction time of 40 min. The leaching process essentially reached equilibrium within 80 min. Thereafter, increasing the leaching time resulted in a small increase in the leaching rates of rubidium and potassium, while the increase in leaching time resulted in a reduction in equipment capacity and an increase in production costs. Therefore, considering the actual production situation, the optimum leaching time was determined to be 80 min.

3.3.4. Effect of the liquid-to-solid ratio

From a kinetic point of view, an increase in the liquid-to-solid ratio reduces the viscosity of the slurry and facilitates an increase in mass transfer efficiency [40]. As shown in Fig. 7(d), the leaching rates of rubidium and potassium increased with increasing liquid-to-solid ratios under the constant conditions of an initial NaOH concentration of 200 g/L, leaching temperature of 95°C, leaching time of 80 min, and stirring rate of 400 r/min. When the liquid-to-solid ratio was 3 mL/g, the leaching rates for both rubidium and potassium were low at 72.93% and 64.59% respectively. The reason was that when the liquid-to-solid ratio was small, the viscosity of the solution was large and the contact between minerals and alkali was insufficient, resulting in a poor leaching rate. As the liquid-to-solid ratio gradually increased, the mass transfer rate between the Slag-1 and the alkali solution continued to increase. In particular, when the liquid-to-solid ratio was increased to 5 mL/g, the leaching rates of rubidium and potassium reached 97.56% and 95.23% respectively. Thereafter, the leaching rate of the metals almost ceased to change when the liquid-to-solid ratio continued to be increased. Considering the cost factor, the optimum liquid-to-solid ratio was chosen to be 5 mL/g.

The XRD patterns (Fig. 10) of the leaching residue obtained at different liquid-to-solid ratios were further analyzed. When the liquid-to-solid ratio was 3 mL/g, the leaching residue was in an amorphous state. As the liquid-to-solid ratio increased, the intensity of the sodalite peak increased, eventually forming a sodalite phase with a stronger peak at a liquid-to-solid ratio of 5 mL/g. Finally, when the liquid-to-solid ratio was increased to 10 mL/g, a small amount of hydrated calcium silicate appeared in the leaching residue, which may be related to the increase in the total amount of alkali.

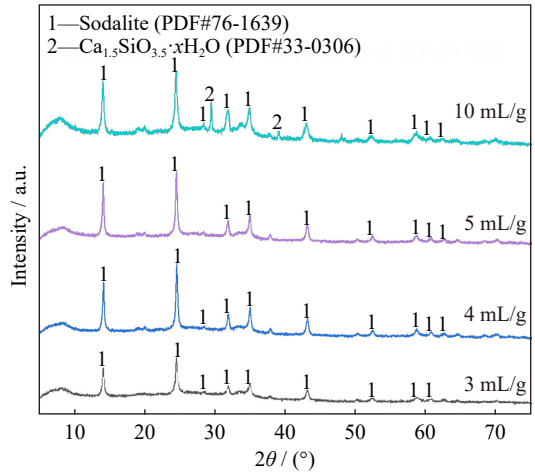

Fig. 10. XRD patterns of the leaching residue at various liquid-to-solid ratios.

By systematic experiments, the optimum leaching conditions were determined to be an initial NaOH concentration of 200 g/L, a leaching temperature of 95°C, a liquid-to-solid ratio of 5 mL/g, a reaction time of 80 min, a stirring rate of 400 r/min. Under the optimum mineral dissociation and leaching conditions, the yields of rubidium and potassium were 97.56% and 95.23%, respectively. Rubidium and potassium in the leachate can be further separated by solvent extraction to obtain RbCl and KCl. The separation of rubidium and potassium by solvent extraction has been systematically studied by our group previously, with approximately 98% of the rubidium being extracted from the alkali leaching solution using t-BAMBP (Tables S2 and S3) [31,41].

Finally, the morphology of the Slag-1 and leaching residue obtained under optimum conditions was also compared, and SEM–EDS images are shown in Fig. 11. The Slag-1 had a large particle size and consisted of a lumpy structure with a smooth surface. However, the lumpy structure of the Slag-1 was destroyed by alkali leaching. The leaching residue formed was made up of a large number of small balls with rough surfaces and regular shapes gathered together.

3.4. Desilication of alkaline leaching liquor

Approximately 35wt% of the silicon (15 g/L) was also leached into the solution during the alkali leaching process. The silicon in the leachate was easily crystallized and precipitated, causing consumption of alkali and detrimental effects on rubidium extraction during solvent extraction. Therefore,

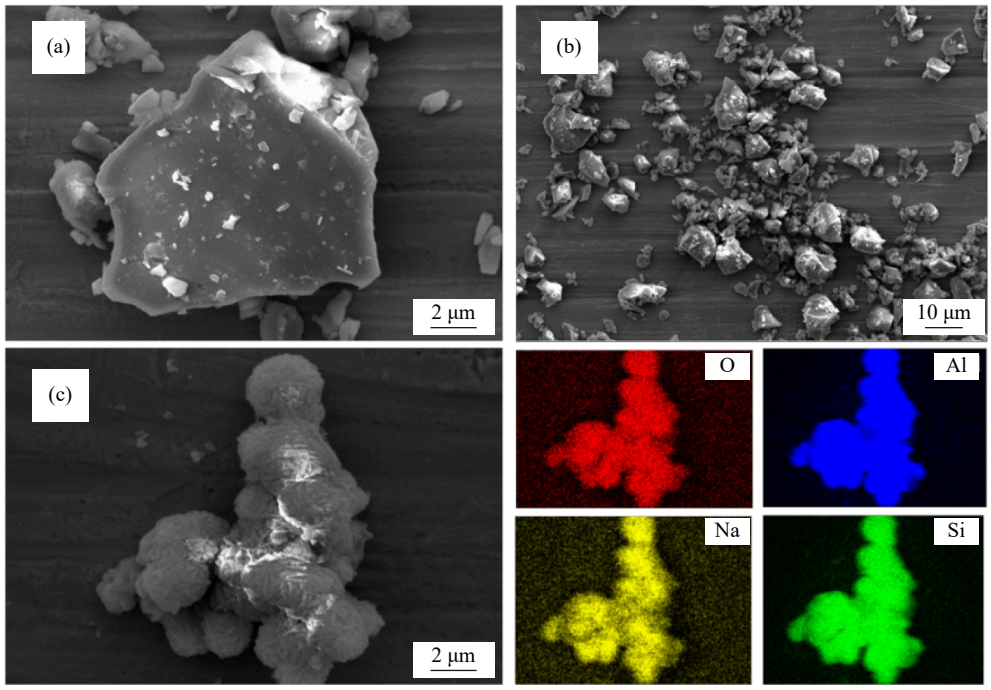

Fig. 11. (a, b) SEM images of Slag-1 at different magnifications and (c) SEM image and EDS maps of leaching residue under optimum conditions.

the dissolved silicon must be removed to purify the leachate. The most common method for desilication of leach liquor was to add CaO for desilication. However, if CaO was added to the process for desalination, a low utilization value of wollastonite would be produced. To achieve high-value utilization of silicon and a small number of aluminum resources in the leachate, $Al(OH)_3$ was added to the leachate to supplement the aluminum source for desilication treatment [42–43]. The effect of the addition of $Al(OH)_3$ on the effectiveness of desilication was investigated systematically. The desilication temperature, desilication time, and stirring rate were kept at 95°C, 80 min, and 500 r/min respectively, which were the same as the optimum leaching conditions of the Slag-1. The main chemical reactions occurring during the addition of $Al(OH)_3$ to the leachate for desilication were shown in Eqs. (3)–(5).

$$Al(OH)_3 + OH^- = Al(OH)_4^- \quad (3)$$

$$H_2SiO_4^{2-} + 2Al(OH)_4^- \rightleftarrows [Al_2[H_2SiO_4](OH)_6]^{2-} + 2OH^- \quad (4)$$

$$7Na^+ + 6[Al_2[H_2SiO_4](OH)_6]^{2-} \rightleftarrows 3[Na_2O \cdot Al_2O_3 \cdot 2SiO_2] \cdot NaAl(OH)_4 \cdot nH_2O + 5Al(OH)_4^- + (12-n)H_2O \quad (5)$$

As shown in Fig. 12(a), the extent of desilication was strengthened as the molar ratio of $Al(OH)_3$ to SiO_2 increased. When $Al(OH)_3$ was added at 1.75 times the amount of dissolved silica, the precipitation rate of silica reached a maximum of approximately 94%. Hence, the optimum dosage of $Al(OH)_3$ was determined to be a molar ratio of $Al(OH)_3$ to SiO_2 of 1.75. Fig. 12(b) shows the XRD pattern of the Slag-2. The main phases of the Slag-2 were sodalite and sodium aluminum silicate hydrate. When the molar ratio of $Al(OH)_3$ to SiO_2 was 1.75, most of the sodium aluminum silicate hydrate was transformed into sodalite with a rough surface (Fig. S1).

As a typical mineral of the zeolite group, sodalite has the same β characteristic cage structure as zeolite, which can also be further synthesized by zeolite transformation methods [44]. Zeolites have excellent adsorption, ion exchange, and catalytic properties, and the technology for synthesizing zeolites with sodalite as raw material is well matured

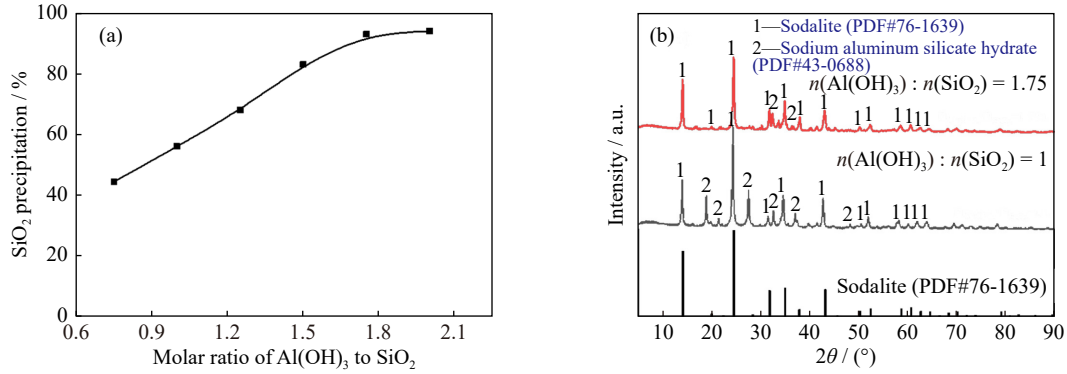

Fig. 12. (a) Effect of dosage of $Al(OH)_3$ on the desilication and (b) XRD patterns of the Slag-2 (desilication temperature = 95°C; desilication time = 80 min). *n*(x) represents the amount of substance (mole) of x.

[45–46]. After pretreatment of the leaching residue obtained under the comprehensive experiment, the leaching residues were successfully synthesized into zeolite A (Fig. S2) by controlling $n(SiO_2)$: $n(Al_2O_3)$ = 1, $n(H_2O)$: $n(Na_2O)$ = 74, and $n(Na_2O)$: $n(SiO_2)$ = 1.7 at a temperature of 100°C for 12 h.

The results of the desilication experiments showed that the addition of activated $Al(OH)_3$ to the leaching solution under the same conditions as the optimum leaching temperature and leaching time gave a good desilication effect, and the leaching residue and the Slag-2 were both sodalites. Therefore, to further simplify the process, the optimal amount of activated $Al(OH)_3$ was added during alkaline leaching so that leaching and desilication could be carried out simultaneously, with the results shown in Table 2.

Table 2. Leaching results under comprehensive conditions

Component	Rb	K	Si	Al	Fe	Ca	F
Leaching rate / %	98.67	96.23	1.8	13.6	<1	<1	96
Content / ($g \cdot L^{-1}$)	0.25	8.65	0.48	1.7	<0.01	<0.01	2.5

The leaching rates of rubidium and potassium remained above 95% under the combined experimental conditions and the leaching rate of silicon was reduced to 1.8% from the previous 35%.

3.5. Proposed process route and cost analysis

Previous exploratory experiments also explored the feasibility of the sodiumization roasting–water leaching process and the direct roasting–alkali leaching process for the treatment of rubidium ores. It was found that even if the amount of NaOH in the roasting stage was increased, little rubidium was leached in the water leaching stage. If direct roasting was carried out without the addition of NaOH, the leaching rate of rubidium during alkali leaching was only approximately 55% even if the initial concentration of NaOH reached 300 g/L and the temperature was 100°C. It also demonstrated the important role of the addition of small amounts of NaOH during the roasting stage in the reconstitution of the mineral phase.

After a comparison of the various processes currently available for the treatment of complex rubidium ores, based on our group's works on the separation of rubidium and potassium from alkaline solutions [31,41]. The proposed flow chart for the treatment of complex rubidium ores is shown in Fig. 13.

The potential economic value was conducted for treating 1 t of rubidium ore by the proposed method in China (Table S4). The prices of various products come from the latest data on the Internet [47–48]. In addition, energy and equipment costs are calculated with reference to Ref. [48]. The economic analysis is based on the market situations in China and there will be some differences in other countries.

Table S4 shows that the profit of treating is approximately 1.41 million yuan. In addition, if the cost of 1 t of rubidium ore is calculated at 60% of the rubidium, potassium, silicon, and aluminum contained in it, the cost of raw material is

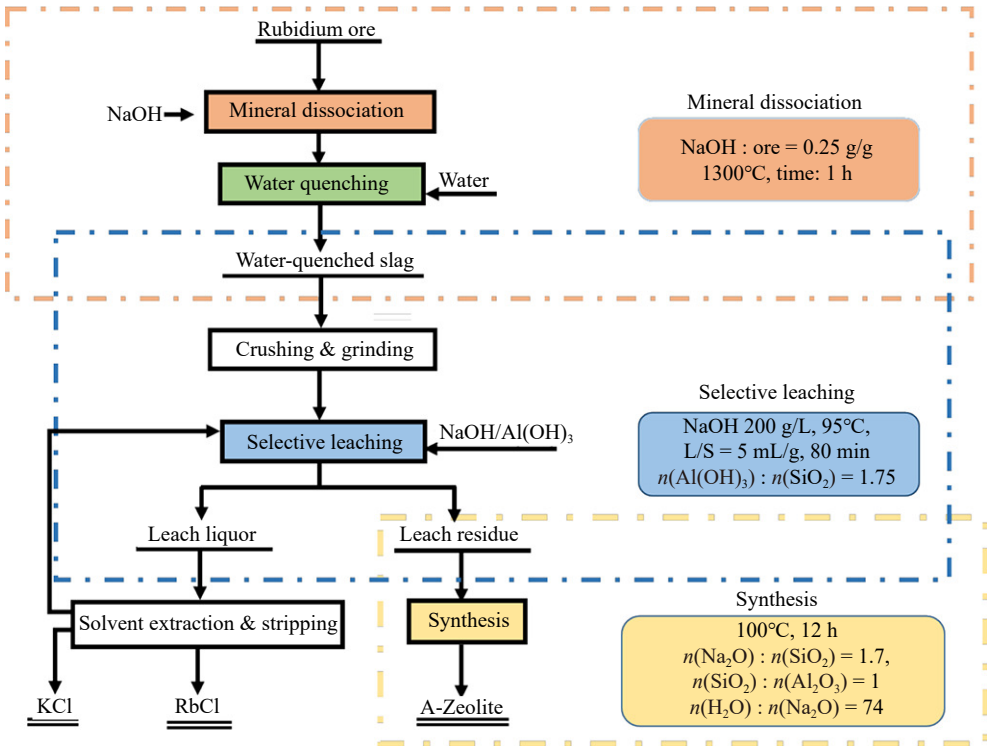

Fig. 13. Flow chart of comprehensive utilization of rubidium ore resources.

about 0.86 million yuan. Through calculation, it can be concluded that the final profit is about 553599 yuan, indicating that the new method proposed has considerable economic benefits.

4. Conclusions

An efficient process for the comprehensive utilization of rubidium ore resources was proposed, the following conclusions were drawn.

(1) By mineral dissociation, the stable silicon–oxygen tetrahedra in the rubidium ore were disrupted, the rubidium was released and the thermal activated slag (Slag-1) existed in a highly reactive, amorphous state. The optimum dissociation conditions were as follows: a ratio of NaOH to rubidium ore of 25wt%, a dissociation temperature of 1300°C, a roasting time of 1 h. Under these conditions, the highest leaching activity of the Slag-1 was obtained.

(2) The Slag-1 was treated by selective leaching at an initial NaOH concentration of 200 g/L, a leaching temperature of 95°C, a leaching time of 80 min, and a liquid-to-solid ratio of 5 mL/g to achieve maximum leaching rates of 97.56% and 95.23% for rubidium and potassium, respectively.

(3) Desilication was carried out by adding $Al(OH)_3$ to the leaching solution under optimal leaching conditions. When $Al(OH)_3$ was added at 1.75 times the amount of dissolved silica, the leaching rates of rubidium and potassium were 98.67% and 96.23% respectively, while only 1.8% of silicon entered the solution, simplifying the process.

(4) Moreover, the leaching residue and the Slag-2 were sodalites, which were successfully synthesized to zeolite A by hydrothermal conversion.

Acknowledgements

This work was financially supported by the National Natural Science Foundation of China (Nos. U1802253 and 52034002), and the Fundamental Research Funds for the Central Universities,China (No. FRF-TT-19-001).

Conflict of Interest

The authors declare that they have no known competing financial interests or personal relationships that could have appeared to influence the work reported in this paper.

Supplementary Information

The online version contains supplementary material available at https://doi.org/10.1007/s12613-022-2436-1.

References

[1] L.O. Quarrie, The effects of atomic rubidium vapor on the performance of optical windows in diode pumped alkali lasers (DPALs), *Opt. Mater.*, 35(2013), No. 5, p. 843.

[2] S.S. Losev, D.I. Sevostianov, V.V. Vassiliev, and V.L. Velishansky, Production of miniature glass cells with rubidium for chip scale atomic clock, *Phys. Procedia*, 71(2015), p. 242.

[3] P.C. Harikesh, H.K. Mulmudi, B. Ghosh, *et al*., Rb as an alternative cation for templating inorganic lead-free perovskites for solution processed photovoltaics, *Chem. Mater.*, 28(2016), No. 20, p. 7496.

[4] S. Wang, R.X. Ma, C.Y. Wang, S.N. Li, and H. Wang, Incorporation of Rb cations into Cu_2FeSnS_4 thin films improves structure and morphology, *Mater. Lett.*, 202(2017), p. 36.

[5] M. Saliba, T. Matsui, K. Domanski, *et al*., Incorporation of rubidium cations into perovskite solar cells improves photovoltaic performance, *Science*, 354(2016), No. 6309, p. 206.

[6] L.F. Wang, M.M. Geng, X.N. Ding, *et al*., Research progress of the electrochemical impedance technique applied to the high-capacity lithium-ion battery, *Int. J. Miner. Metall. Mater.*, 28(2021), No. 4, p. 538.

[7] N. Vieceli, C.A. Nogueira, M.F.C. Pereira, *et al*., Effects of mechanical activation on lithium extraction from a lepidolite ore concentrate, *Miner. Eng.*, 102(2017), p. 1.

[8] H. Guo, G. Kuang, J.X. Yang, and S. Hu, Fundamental research on a new process to remove Al^{3+} as potassium alum during lithium extraction from lepidolite, *Metall. Mater. Trans. B*, 47(2016), No. 6, p. 3557.

[9] Z.Q. Shan, X.Q. Shu, J.F. Feng, and W.N. Zhou, Modified calcination conditions of rare alkali metal Rb-containing muscovite ($KAl_2[AlSi_3O_{10}](OH)_2$), *Rare Met.*, 32(2013), No. 6, p. 632.

[10] M.R. Tavakoli Mohammadi, S.M. Javad Koleini, S. Javanshir, H. Abolghasemi, and M. Abdollahy, Extraction of rubidium from gold waste: Process optimization, *Hydrometallurgy*, 151(2015), p. 25.

[11] X.H. Guo, M.P. Zheng, X.F. Liu, Z. Nie, and L. Pu, Saline cesium resource and prospect of its exploitation and utilization in Tibet, *J. Salt .Chem. Ind.*, 37(2008), p. 24.

[12] T. Nur, G. Naidu, P. Loganathan, J. Kandasamy, and S. Vigneswaran, Rubidium recovery using potassium cobalt hexacyanoferrate sorbent, *Desalin. Water Treat.*, 57(2016), No. 55, p. 26577.

[13] Y.S. Liao and D.J. Yang, Application status of rubidium resource and research situation of its extraction technology, *Yunnan Metall.*, 41(2012), No. 4, p. 27.

[14] G. Naidu, P. Loganathan, S. Jeong, *et al*., Rubidium extraction using an organic polymer encapsulated potassium copper hexacyanoferrate sorbent, *Chem. Eng. J.*, 306(2016), p. 31.

[15] M.S. Safarzadeh, M.S. Moats, and J.D. Miller, Acid bake-leach process for the treatment of enargite concentrates, *Hydrometallurgy*, 119-120(2012), p. 30.

[16] P. Meshram, Abhilash, B.D. Pandey, T.R. Mankhand, and H. Deveci, Acid baking of spent lithium ion batteries for selective recovery of major metals: A two-step process, *J. Ind. Eng. Chem.*, 43(2016), p. 117.

[17] S.L. Zheng, P. Li, L. Tian, *et al*., A chlorination roasting process to extract rubidium from distinctive Kaolin ore with alternative chlorinating reagent, *Int. J. Miner. Process.*, 157(2016), p. 21.

[18] Q.X. Yan, X.H. Li, Z.X. Wang, *et al*., Extraction of lithium from lepidolite by sulfation roasting and water leaching, *Int. J. Miner. Process.*, 110-111(2012), p. 1.

[19] C. Yang, J.L. Zhang, Q.K. Jing, Y.B. Liu, Y.Q. Chen, and C.Y. Wang, Recovery and regeneration of $LiFePO_4$ from spent lithium-ion batteries via a novel pretreatment process, *Int. J. Miner. Metall. Mater.*, 28(2021), No. 9, p. 1478.

[20] P. Xing, C.Y. Wang, B.Z. Ma, L. Wang, W.J. Zhang, and Y.Q. Chen, Rubidium and potassium extraction from granitic rubidium ore: Process optimization and mechanism study, *ACS Sustainable Chem. Eng.*, 6(2018), No. 4, p. 4922.

[21] Q. Zeng, S.Z. Li, W. Sun, L. Hu, H. Zhong, and Z.G. He, Eco-

friendly leaching of rubidium from biotite-containing minerals with oxalic acid and effective removal of Hg^{2+} from aqueous solution using the leaching residues, *J. Cleaner Prod.*, 306(2021), art. No. 127167.

[22] H. Xu and J.S.J. van Deventer, The effect of alkali metals on the formation of geopolymeric gels from alkali-feldspars, *Colloids Surf. A*, 216(2003), No. 1-3, p. 27.

[23] B.E. Kalinowski and P. Schweda, Kinetics of muscovite, phlogopite, and biotite dissolution and alteration at pH 1–4, room temperature, *Geochim. Cosmochim. Acta*, 60(1996), No. 3, p. 367.

[24] D. Ciceri, M. de Oliveira, R.M. Stokes, T. Skorina, and A. Allanore, Characterization of potassium agrominerals: Correlations between petrographic features, comminution and leaching of ultrapotassic syenites, *Miner. Eng.*, 102(2017), p. 42.

[25] K.H. Park, H.I. Kim, P.K. Parhi, *et al*., Extraction of metals from Mo–Ni/Al_2O_3 spent catalyst using H_2SO_4 baking-leaching-solvent extraction technique, *J. Ind. Eng. Chem.*, 18(2012), No. 6, p. 2036.

[26] Y.M. Chen, N.N. Liu, L.G. Ye, S. Xiong, and S.H. Yang, A cleaning process for the removal and stabilisation of arsenic from arsenic-rich lead anode slime, *J. Cleaner Prod.*, 176(2018), p. 26.

[27] Z. Luo, J. Yang, H.W. Ma, M.T. Liu, and X. Ma, Recovery of magnesium and potassium from biotite by sulfuric acid leaching and alkali precipitation with ammonia, *Hydrometallurgy*, 157(2015), p. 188.

[28] N. Harouiya and E.H. Oelkers, An experimental study of the effect of aqueous fluoride on quartz and alkali-feldspar dissolution rates, *Chem. Geol.*, 205(2004), No. 1-2, p. 155.

[29] S. Nisan, F. Laffore, C. Poletiko, and N. Simon, Extraction of rubidium from the concentrated brine rejected by integrated nuclear desalination systems, *Desalin. Water Treat.*, 8(2009), No. 1-3, p. 236.

[30] Q. Zeng, L.M. Huang, D.X. Ouyang, Y.H. Hu, H. Zhong, and Z.G. He, Process optimization on the extraction of rubidium from rubidium-bearing biotite, *Miner. Eng.*, 137(2019), p. 87.

[31] Y.W. Lv, P. Xing, B.Z. Ma, *et al*., Efficient extraction of lithium and rubidium from polylithionite via alkaline leaching combined with solvent extraction and precipitation, *ACS Sustainable Chem. Eng.*, 8(2020), No. 38, p. 14462.

[32] P. Xing, C.Y. Wang, L. Zeng, *et al*., Lithium extraction and hydroxysodalite zeolite synthesis by hydrothermal conversion of α-spodumene, *ACS Sustainable Chem. Eng.*, 7(2019), No. 10, p. 9498.

[33] G. Martin, C. Pätzold, and M. Bertau, Integrated process for lithium recovery from zinnwaldite, *Int. J. Miner. Process.*, 160(2017), p. 8.

[34] X. Ma, J. Yang, H.W. Ma, and C.J. Liu, Hydrothermal extraction of potassium from potassic quartz syenite and preparation of aluminum hydroxide, *Int. J. Miner. Process.*, 147(2016), p. 10.

[35] Z.Q. Zhang and R.Z. Yuan, Study on dehydroxylation process of kaolinite and its structural change, *Bull. Chin. Ceram. Soc.*, 1993, No. 6, p. 37.

[36] S.Q. Su, H.W. Ma, and X.Y. Chuan, Hydrothermal decomposition of K-feldspar in KOH–NaOH–H_2O medium, *Hydrometallurgy*, 156(2015), p. 47.

[37] M.K. Naskar, D. Kundu, and M. Chatterjee, Effect of process parameters on surfactant-based synthesis of hydroxy sodalite particles, *Mater. Lett.*, 65(2011), No. 3, p. 436.

[38] N.N. Xue, Y.M. Zhang, T. Liu, J. Huang, and Q.S. Zheng, Effects of hydration and hardening of calcium sulfate on muscovite dissolution during pressure acid leaching of black shale, *J. Cleaner Prod.*, 149(2017), p. 989.

[39] N. Vieceli, F.O. Durão, C. Guimarães, C.A. Nogueira, M.F.C. Pereira, and F. Margarido, Kinetic approach to the study of froth flotation applied to a lepidolite ore, *Int. J. Miner. Metall. Mater.*, 23(2016), No. 7, p. 731.

[40] H. Li, J. Eksteen, and G. Kuang, Recovery of lithium from mineral resources: State-of-the-art and perspectives - A review, *Hydrometallurgy*, 189(2019), art. No. 105129.

[41] P. Xing, C.Y. Wang, L. Wang, B.Z. Ma, Y.Q. Chen, and G.D. Wang, Clean and efficient process for the extraction of rubidium from granitic rubidium ore, *J. Cleaner Prod.*, 196(2018), p. 64.

[42] L.M. Zeng and Z.B. Li, Solubility and modeling of sodium aluminosilicate in NaOH–$NaAl(OH)_4$ solutions and its application to desilication, *Ind. Eng. Chem. Res.*, 51(2012), No. 46, p. 15193.

[43] L.N. Shi, S. Ruan, J. Li, and A.R. Gerson, Desilication of low alumina to caustic liquor seeded with sodalite or cancrinite, *Hydrometallurgy*, 170(2017), p. 5.

[44] X.D. Liu, Y.P. Wang, X.M. Cui, Y. He, and J. Mao, Influence of synthesis parameters on NaA zeolite crystals, *Powder Technol.*, 243(2013), p. 184.

[45] P. Xing, C.Y. Wang, B.Z. Ma, and Y.Q. Chen, Removal of Pb(II) from aqueous solution using a new zeolite-type absorbent: Potassium ore leaching residue, *J. Environ. Chem. Eng.*, 6(2018), No. 6, p. 7138.

[46] L.L. Bai, K.X. Li, Y.B. Yan, X.L. Jia, J.M. Lee, and Y.H. Yang, Catalytic epoxidation of *cis*-cyclooctene over vanadium-exchanged faujasite zeolite catalyst with ionic liquid as cosolvent, *ACS Sustainable Chem. Eng.*, 4(2016), No. 2, p. 437.

[47] H. Jin, J.L. Zhang, D.D. Wang, Q.K. Jing, Y.Q. Chen, and C.Y. Wang, Facile and efficient recovery of lithium from spent $LiFePO_4$ batteries via air oxidation-water leaching at room temperature, *Green Chem.*, 24(2022), No. 1, p. 152.

[48] D. Hu, B.Z. Ma, X. Li, *et al*., Efficient separation and recovery of gallium and indium in spent CIGS materials, *Sep. Purif. Technol.*, 282(2022), art. No. 120087.